

Model for Radiation Contamination by Outgassing from Space Platforms

Stephen J. Young* and Ronald R. Herm†
The Aerospace Corporation, El Segundo, California

Infrared sensors mounted on space platforms (e.g., Space Shuttle and satellites) may be subject to infrared radiation contamination from molecular gases released from the platform itself. Models for order-of-magnitude estimates of the contamination level caused by this effect are formulated. The mechanisms for vibrational excitation of the ejected species include 1) thermal excitation at the platform surface, 2) absorption of solar and Earthshine radiation, and 3) collisions with ambient atmospheric species. The model is applied to estimate the effects that the outgassing of H₂O from the Shuttle environment would have on the CIRRIS 1A Earth-limb radiance mission. Results indicate that for outgassing rates less than $\sim 10^{21}$ molecules/s and Shuttle altitudes above ~ 300 km, detection in the 2.7- μ m spectral region would be only slightly degraded, but that detection around 6.3 μ m may be seriously impaired by the mechanism of absorption and re-emission of Earthshine radiation by the H₂O contamination molecules.

I. Introduction

THE performance of infrared sensing systems mounted on low-Earth-orbit platforms can be degraded by contaminant gases that originate from the ambient atmosphere or from the platform itself.¹ Two mechanisms that seriously interfere with sensor design performance are 1) condensation of contaminants on the cryogenically cooled optical elements of the sensor telescope, and 2) radiation in the sensor field of view from infrared-active contaminant species. The second of these effects is treated in this work. Simple analytical models are developed for estimating order-of-magnitude radiation levels. The models are developed with the Space Shuttle as the space platform, the CIRRIS 1A Earth-limb-scanning telescope as the sensing system, and H₂O as the contaminant species, but the methods can be readily applied to other situations.

The CIRRIS 1A program is being carried out by the Air Force Geophysics Laboratory, Hanscom Air Force Base, Mass. There is no formal reference to this program. The predecessor project CIRRIS is described in Ref. 2.

Water is one of the most important of the contaminant species generated by the Shuttle. Outgassing from the exterior Shuttle surfaces, and bay area, thruster firing, and venting from the Shuttle interior, all contribute to the ejection of H₂O molecules. The principal infrared emissions from H₂O occur in the 2.7- and 6.3- μ m regions and arise from the vibrational stretching and bending modes, respectively. Spectroscopic parameters used in this work are listed in Table 1.

Three relatively separate mechanisms for the excitation of molecular vibration (and hence infrared radiation) can be heuristically identified: 1) Molecules ejected from Shuttle surfaces can carry a degree of thermal vibrational excitation characterized by the surface temperature. 2) After ejection, H₂O molecules can be vibrationally excited by absorbing solar or Earthshine radiation. 3) Molecules of H₂O may be vibrationally excited in energetic collisions with ambient atmospheric species (primarily oxygen atoms at Shuttle altitudes of

200–600 km). The energy of excitation here derives from the orbital speed of the Shuttle through the atmosphere, $v_o \approx 8$ km/s.

This paper begins with a discussion of the CIRRIS 1A sensors, followed by two sections that treat the radiation models. In Sec. III, expressions are derived for the total power radiated by ejected H₂O molecules into the sensor apertures; Sec. IV considers the spectral efficiency of the sensors for detecting this radiation. Sections V and VI discuss the magnitude of H₂O ejection from the Shuttle and present the results.

II. CIRRIS 1A Sensors

The sensors of CIRRIS 1A include an interferometer spectrometer and a multifiltered radiometer capable of sensing H₂O radiation at 2.7 and 6.3 μ m. The average operating capabilities of the sensors are summarized in Table 2.

Photon detection by the sensors differs, depending on whether emission occurs in the near field or far field of the sensor. For a source on the optical axis, an emitted photon will be detected only if it enters the sensor aperture at an angle less than $\alpha \approx (\Omega/\pi)^{1/2}$. This is the half-angle of the field-of-view cone Ω . Photons emitted from a distance greater than $z_s \approx (a/\Omega)^{1/2}$ will, of necessity, do so at an angle less than α if they are to be detected. This is the far field, and the probability that a photon from an isotropic emission source is detected is

$$p(z) = \frac{1}{2} [1 - z/(z^2 + a/\pi)^{1/2}] \approx \frac{1}{4\pi} \frac{a}{z^2} \quad (1a)$$

The approximate form given is good to better than 1% when $\Omega \leq 0.042$ sr and is used here. Photons emitted from a distance less than z_s will be detected only if they emit into a solid angle Ω directed toward the sensor. For an isotropic source, the probability of detection in this near field is then

$$p(z) = \frac{\Omega}{4\pi} \quad (1b)$$

Later, this probability will be needed for a source that is extended exponentially along the optical axis; i.e. a source whose strength varies as $e^{-z/L}$, where L is the mean emission distance. The average of $p(z)$ over the exponential distribution is

$$\bar{p} = \int_0^\infty p(z) \frac{e^{-z/L}}{L} dz = \frac{\Omega}{4\pi} F(\alpha) \quad (2)$$

Presented as Paper 87-0102 at the AIAA 25th Aerospace Sciences Meeting, Reno, NV, Jan. 12–15, 1987; received Nov. 13, 1987; revision received April 16, 1988. Copyright © American Institute of Aeronautics and Astronautics, Inc., 1987. All rights reserved.

*Research Physicist, Infrared Sciences Department.

†Head, Infrared Sciences Department, Chemistry and Physics Laboratory.

Table 1 Spectroscopic parameters for H₂O

| Parameter | Mode | |
|-------------|------|---------|
| | Bend | Stretch |
| λ_c | 6.3 | 2.7 |
| ν_c | 1600 | 3760 |
| A | 19 | 83 |
| A_r | | 0.3 |
| B | | 27.3 |
| | | 14.6 |
| | | 9.5 |
| \bar{B} | | 17.1 |
| ω | 310 | 260 |

λ_c = band wavelength (μm); ν_c = band center (cm^{-1}); A = vibrational transition probability (s^{-1}); A_r = rotational transition probability (s^{-1}); B = rotational constants (cm^{-1}); \bar{B} = average rotational constant (cm^{-1}); ω = mean emission bandwidth at 300 K (cm^{-1}).

Table 2 Sensor optical parameters^a

| Interferometer | |
|---|--|
| $a = 161 \text{ cm}^2$ | |
| $\Omega = 1.0 \times 10^{-4} \text{ sr}$ | |
| $z_s = 13 \text{ m}$ | |
| $\Delta\nu = 4 \text{ cm}^{-1}$ | |
| NESR = $6.8 \times 10^{-12} \text{ W/cm}^2\text{-sr}$ at $2.7\text{-}\mu\text{m}$ | |
| NESR = $2.6 \times 10^{-13} \text{ W/cm}^2\text{-sr}$ at $6.3\text{-}\mu\text{m}$ | |
| Radiometer | |
| $a = 184 \text{ cm}^2$ | |
| $\Omega = 1.5 \times 10^{-6} \text{ sr}$ | |
| $z_s = 110 \text{ m}$ | |
| $\Delta\nu = 4000 - 2940 = 1060 \text{ cm}^{-1}$ for $2.7\text{-}\mu\text{m}$ filter | |
| $\Delta\nu = 1670 - 1090 = 580 \text{ cm}^{-1}$ for $6.3\text{-}\mu\text{m}$ filter | |
| NESR = $1.5 \times 10^{-10} \text{ W/cm}^2\text{-sr}$ for $2.7\text{-}\mu\text{m}$ filter | |
| NESR = $2.6 \times 10^{-11} \text{ W/cm}^2\text{-sr}$ for $6.3\text{-}\mu\text{m}$ filter | |

a = effective entrance aperture area; Ω = field of view; z_s = dividing point between near and far field of sensor; $\Delta\nu$ = spectral resolution; NESR = noise-equivalent sensor radiance.

^aSource: CIRRUS 1A Critical Design Review, Space Dynamics Laboratory, University of Utah, Logan, UT, April 27-28, 1983.

where

$$\alpha = \frac{1}{L} (a/\Omega)^{1/2}$$

$$F(\alpha) = 1 - e^{-\alpha} + \alpha E_2(\alpha)$$

$$E_2(\alpha) = \text{exponential integral}$$

$F(\alpha)$ is plotted in Fig. 1. The asymptotic limits are $F(\alpha) \sim 2\alpha$ as $\alpha \rightarrow 0$ (far-field limit) and $F(\alpha) \sim 1 - 2e^{-\alpha}/\alpha$ as $\alpha \rightarrow \infty$ (near-field limit).

III. Radiation Models

A model of radiation contamination consisting of three relatively separate molecular excitation mechanisms was developed (Fig. 2). For each contribution, the initial step is the ejection of a water molecule from the Shuttle surface. The molecule is assumed to originate from a point source, to be ejected uniformly into the 2π hemisphere containing the sensor field of view, and not to interact with any other ejected molecules. The ejection speed is taken as constant and equal to the mean molecular speed at the temperature of the Shuttle environment,

$$v_e = (8RT_s/\pi m)^{1/2} \quad (3)$$

Here, a Shuttle surface temperature of $T_s \approx 300 \text{ K}$ is used, and gives $v_e \approx 5.9 \times 10^4 \text{ cm/s}$ for a molecular mass of $m = 18 \text{ g}$

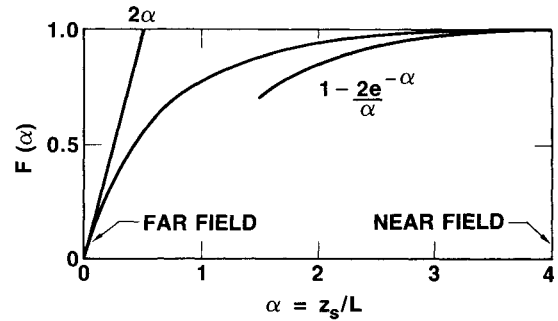


Fig. 1 Photon detection function.

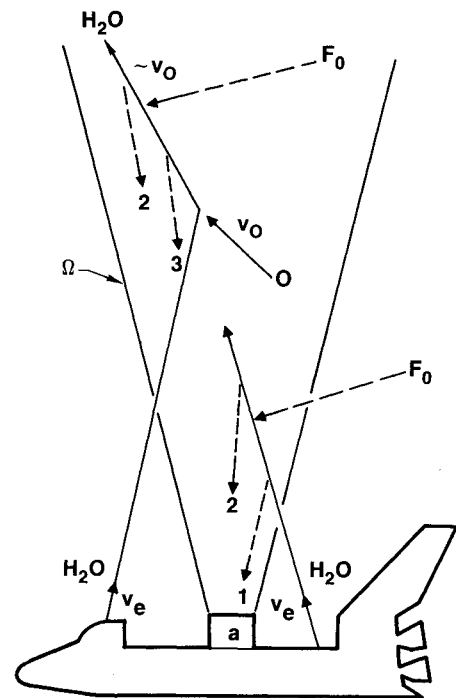


Fig. 2 Radiation contamination contributions. Emission by molecules excited 1) at Shuttle surface, 2) by solar and Earthshine radiation, and 3) by collisions with atomic oxygen.

mole. R is the gas constant $8.3143 \times 10^7 \text{ erg/K-mole}$. The error introduced by using this mean-speed approximation rather than the full velocity distribution around the mean speed was estimated to be less than 20%. For this ejection model, the H₂O number density around the point of ejection is

$$n(z) = \frac{M}{2\pi v_e z^2} \quad (4)$$

where z is the radial coordinate and M is the molecular ejection rate into a hemisphere (molecules/s). The magnitude of M is considered in Sec. IV.

The radiation mechanism treated in Sec. III.A involves a water molecule that is vibrationally excited at the Shuttle surface, is ejected from the surface, and subsequently radiates by spontaneous emission. At the ejection velocity previously quoted, and with the transition probabilities of Table 1, the characteristic length for radiation by H₂O is 7-30 m. This dimension is comparable to Shuttle dimensions, but large enough to ensure that the assumption of a point source of ejection does not introduce an error of more than a factor of ~ 2 . The radiation mechanism discussed in Sec. III.B involves collisions of ejected H₂O molecules with ambient atmospheric species.

At the lowest Shuttle altitude considered here (200 km), the ambient mean free path is $L \approx 240$ m. In the time that it takes an ejected molecule to travel this distance through the ambient atmosphere at orbital velocity v_o , it will move a distance $L_e = (v_e/v_o)L \approx 18$ m from the source. Again, this distance is comparable to Shuttle dimensions so that the point source assumption is no worse than a factor of ~ 2 in accuracy. At an altitude of 300 km, the point source assumption introduces negligible error for this radiation mechanism.

A. Radiation Excitation Model

The principal mechanism for exciting radiation in the model is the absorption and re-emission of solar and Earthshine radiation. The solution to be presented for this mechanism is obtained by solving a first-order differential equation. The boundary condition required to complete the solution is the degree of vibrational excitation at the Shuttle surface; thus, this model accounts for two of the heuristic radiation contributions.

In this model, a vibration-rotation emission band is treated as arising from a simple two-level system representing the upper and lower vibrational levels of the transition. No account is made here of the distribution over rotational levels that establishes the width of the band. Considerations of bandwidth are made in the next section. The rate equations governing the relative populations of the upper and lower level in a radiation field are

$$\begin{aligned} v_e \left(\frac{dn_1}{dz} + \frac{2n_1}{z} \right) &= -n_1 G_{10} + n_0 G_{01} \\ v_e \left(\frac{dn_0}{dz} + \frac{2n_0}{z} \right) &= n_1 G_{10} - n_0 G_{01} \end{aligned} \quad (5)$$

where $n_1(z)$ and $n_0(z)$ are the upper and lower level densities and v_e is the ejection velocity. These equations are written in spherical coordinates with the point ejection source as the origin and z as the radial coordinate.

The coefficients G_{10} and G_{01} are defined in terms of the spontaneous transition probability A of the upper level and the incident radiance F_o by

$$\begin{aligned} G_{01} &= CA \\ G_{10} &= (1 + C)A \\ C &= F_o / 2hc^2v^3 \end{aligned} \quad (6)$$

where v is the level separation wavenumber. The degeneracies of the upper and lower levels have been taken as unity. G_{01} accounts for absorption; G_{10} accounts for both spontaneous and stimulated emission.

The incident radiance contribution from solar radiation is approximated by

$$F_s = \frac{\Omega_s}{4\pi} B(v, T_s) \quad (7)$$

where Ω_s is the solid angle subtended by the sun from the Earth (6.79×10^{-5} sr) and T_s is the effective surface temperature of the sun (6000 K). $B(v, T)$ is the Planck radiation function ($\text{W/cm}^2\text{-sr-cm}^{-1}$)

$$B(v, T) = \frac{2hc^2v^3}{e^{hcv/kT} - 1} \quad (8)$$

The Earthshine contribution to F is approximated by

$$F_e = \frac{1}{2} B(v, T_e) \left\{ 1 - \left[1 - \left(\frac{R_e}{R_e + h} \right)^2 \right]^{1/2} \right\} \quad (9)$$

where T_e is the Earth surface temperature (300 K), R_e is the Earth radius (6368 km), and h is the Shuttle altitude. The expression in braces accounts for Earth curvature. For nighttime calculations, $F_o = F_e$; for daytime calculations, $F_o = F_e + F_s$.

With the conservation condition $n_1(z) + n_0(z) = n(z)$ and the boundary condition $n_1 \rightarrow n_1^o$ and $n_0 \rightarrow n_0^o$ as $z \rightarrow 0$, the solution of the rate equations is

$$\begin{aligned} n_1(z) &= n(z) \left[\frac{C}{1+2C} + \left(\rho_o - \frac{C}{1+2C} \right) e^{-(1+2C)Az/v_e} \right] \\ n_0(z) &= n(z) \left[\frac{1+C}{1+2C} - \left(\rho_o - \frac{C}{1+2C} \right) e^{-(1+2C)Az/v_e} \right] \end{aligned} \quad (10)$$

where $\rho_o = n_1^o/(n_1^o + n_0^o)$. For all cases considered here, the level separation v is large enough that $C \ll 1$ and $\rho_o \ll 1$. Then,

$$\begin{aligned} n_1(z) &\approx n(z)[C + (\rho_o - C)e^{-Az/v_e}] \\ n_0(z) &\approx n(z) \end{aligned} \quad (11)$$

The range over which the equilibrium concentration of n_1 changes from the value described by the boundary condition ρ_o to the radiative equilibrium value C is $Az/v_e \approx 7-30$ m.

With this result for $n_1(z)$, the actual radiation model can be formulated as

$$N = \frac{1}{a\Omega} \int_0^\infty n_1(z) A hcv p(z) \Omega z^2 dz \quad (12)$$

where

- $n_1(z)$ = density of excited molecules ($1/\text{cm}^3$), Eq. (11)
- A = spontaneous transition probability ($1/\text{s}$), Table 1
- hcv = photon energy (J)
- $p(z)$ = detection probability, Eq. (1)
- $\Omega z^2 dz$ = elemental emission volume (cm^3)
- a = sensor entrance aperture area (cm^2), Table 2
- Ω = sensor field of view (sr), Table 2
- N = radiance ($\text{W/cm}^2\text{-sr}$)

Evaluation of the integral yields

$$N = M \frac{hcv}{8\pi^2 z_s^2} (Q_S + Q_R) \quad (13)$$

where

$$\begin{aligned} Q_S &= F(x)\rho_o \\ Q_R &= [2\alpha - F(x)]C \\ \alpha &= z_s A / v_e \\ z_s &= (a/\Omega)^{1/2} \end{aligned}$$

Q_S measures the contributions from excitation at the Shuttle surface. Q_R accounts for excitation by absorption of solar and Earthshine radiation. $F(x)$ is the sensor function defined in Eq. (2). ρ_o is the degree of excitation at the Shuttle surface

$$\rho_o \approx e^{-hcv/kT_s} \quad (14)$$

B. Collision-Induced Radiation

Contaminant radiation can be produced by energetic collisions between the ejected H_2O molecules and ambient oxygen atoms (assumed to be the sole constituent of the atmosphere at Shuttle altitudes). The distribution in distance from the Shuttle where these collisions occur is taken as exponential, with mean

Table 3 U.S. standard atmosphere, 1976

| h | n | T | L |
|-----|---------|------|------|
| 200 | 7.18(9) | 855 | 0.24 |
| 300 | 6.51(8) | 976 | 2.6 |
| 400 | 1.06(8) | 996 | 16 |
| 500 | 2.19(7) | 999 | 77 |
| 600 | 5.95(6) | 1000 | 280 |

h = altitude, km; n = number density, cm^{-3} ; T = temperature, K; L = mean free path, km.

collision distance equal to the ambient atmospheric mean free path scaled by the velocity ratio v_e/v_o (see the last paragraph of Section III). The ejected molecules are assumed to thermalize with the atmosphere at first collision—i.e., the H_2O molecules come to rest with respect to the atmosphere and assume its translational temperature. The mean free paths and temperatures for the U.S. Standard 1976 model atmosphere are taken from Ref. 3 and shown in Table 3.

The single-quantum approximation is also invoked so that only one photon (at most) is allowed per ejected H_2O molecule, even though the relative energy of motion at the collision speed of $v_o = 8$ km/s is $\epsilon_o \approx 4.5 \times 10^{-12}$ erg and is sufficient to generate up to six photons in the 2.7- μ m band and 14 photons in the 6.3- μ m band.

The actual probability per collision p_c for photon production was derived using vibrational excitation cross sections from the quantum mechanical calculations of Johnson.⁴ Results obtained with a classical trajectory calculation give results that are higher than these by a factor of 2.9 for the upper level of the 6.3- μ m band and 15 for the upper level of the 2.7- μ m band.^{4,5} With Johnson's cross sections and the hard sphere collision cross section $\sigma \approx 6.0 \times 10^{-15}$ cm² deduced from the U.S. Standard 1976 atmosphere, the excitation probabilities at the relative collision speed of 8 km/s were found to be

$$p_c = \begin{cases} 0.001 & 2.7\text{-}\mu\text{m band} \\ 0.012 & 6.3\text{-}\mu\text{m band} \end{cases} \quad (15a)$$

Results are also presented using the classical cross sections because these are widely used in Air Force Systems studies. The resulting probabilities are

$$p_c = \begin{cases} 0.012 & 2.7\text{-}\mu\text{m band} \\ 0.035 & 6.3\text{-}\mu\text{m band} \end{cases} \quad (15b)$$

The collision-induced radiation is modeled by

$$N = \frac{1}{a\Omega} \int_0^\infty \frac{M\Omega}{2\pi} p_c h\nu p(z) \frac{e^{-z/L_e}}{L_e} dz \quad (16)$$

where

- $M\Omega/2\pi$ = number of molecules ejected into sensor field of view per unit time (1/s)
- $h\nu$ = photon energy (J)
- $p(z)$ = detection probability, Eq. (1)
- $\frac{e^{-z/L_e}}{L_e} dz$ = probability of collision in dz at distance z from point ejection source
- p_c = probability of photon excitation in collision, Eq. (15)
- a = sensor entrance aperture area (cm²), Table 2
- Ω = sensor field of view (sr), Table 2
- N = radiance (W/cm²-sr)

In this formulation, it is assumed that the number of H_2O molecules that are collisionally excited in the sensor field of view but that move out of the field of view (by deflection on collision) before they radiate is balanced by the number of molecules that are excited outside the field of view and move in before they radiate.

Evaluation of the integral gives

$$N = M \frac{h\nu}{8\pi^2 z_s^2} Q_c \quad (17)$$

where

$$Q_c = F(\alpha) p_c$$

$$\alpha = z_s/L_e$$

$$L_e = (v_e/v_o)L$$

$$z_s = (a/\Omega)^{1/2}$$

IV. Emission Bandwidth

The foregoing radiation models give the total power radiated into the sensor aperture but do not account for the overlap of the emission bands and the spectral response of the sensors. To estimate the spectral detection efficiency, the emission bands were approximated as rectangular and described by their band center ν_c and full width ω . The band centers are given in Table 1.

The emission bandwidth varies with the mechanism responsible for establishing the rotational population distribution of the excited molecules. For molecules excited at the Shuttle surface, emission widths appropriate to thermal emission at 300 K were computed from H_2O absorption band model parameters from NASA⁶ and from band model parameters derived from the Air Force Geophysics Laboratory atmospheric line compilation.⁷ The two resulting sets of widths are not entirely consistent, and both results are listed in Table 4. The widths were calculated from

$$\omega = \left[\int k(\nu) d\nu \right]^2 / \int k^2(\nu) d\nu \quad (18)$$

where $k(\nu)$ is the absorption band model parameter and the integrations extend over the full width of the band.

The effective emission widths of H_2O molecules in radiative equilibrium with solar and Earthshine radiation were estimated from results obtained in a separate ongoing program. Briefly, H_2O was modeled as a system of three Σ vibrational levels set up to approximate the lowest energy bending and stretch modes of vibration. A single rotational constant of 17.1 cm⁻¹ (average of the three values for H_2O) was assigned to each level. The only transitions allowed between the levels were those of spontaneous and induced emission and absorption within P and R branches of the vibration-rotation band. Both upper levels were connected to the ground level, but the two upper levels were not connected to each other. Also, within a given vibrational level, rotational levels were allowed to mix only by spontaneous and induced emission and absorption within the pure rotation band. The spontaneous emission probabilities of Table 1 were used.

This system was then placed in a radiation field that approximates solar and Earthshine radiation and allowed to come to equilibrium. The sun was approximated as a 6000 K blackbody sphere of solar radius located 1 AU away. The Earth was approximated as a 300 K blackbody sphere of Earth radius. The model H_2O molecule was situated at an altitude of 300 km above the Earth. Using the equilibrium rotational populations that resulted, emission spectra for the two vibration-rotation bands were generated. Effective widths of these bands were computed as in the previous thermal case [Eq. (18)], but with line strengths replacing the absorption band model parameter. The widths are tabulated in Table 4. For comparison, the temperatures T_R implied by these widths (had the rotational population distributions been thermal) are also tabulated.

The estimation of band emission width for radiation induced by energetic collisions with O atoms is the hardest case. The range indicated in Table 4 (1000 \rightarrow 4000 cm⁻¹) results from a number of estimation procedures. The largest value results if it is assumed that ω scales as $T^{1/2}$ and that the effective collision temperature is $\sim 5 \times 10^4$ K (a value that corresponds to a collision velocity of ~ 8 km/s). This is an unrealistically large value. The lowest value results from an heuristic calculation that places the maximum orbital velocity of the H atoms in the rotating H_2O molecule at the interaction velocity of 8 km/s. A middle value of ~ 2800 cm⁻¹ was obtained using the classical mechanics result of Kolb and Elgin⁸ on the transfer of translational to rotational energy in energetic collisions.

For simplicity, and within the quantitative bounds used in this work, the values $\omega = 260$ and 310 cm⁻¹ were used for the 2.7- and 6.3- μ m emission bands, respectively, for all cases except collisions with O. There, the value $\omega = 1000$ cm⁻¹ was used for both bands.

Table 4 Emission bandwidths

| Excitation mechanism | T _R , K | | ω , cm ⁻¹ | |
|----------------------|----------------------|-------------------|--------------------------------------|--------------------------------------|
| | 2.7- μ m band | 6.3- μ m band | 2.7- μ m band | 6.3- μ m band |
| Shuttle surface | 300 | 300 | 260 ^a 315 ^b | 310 ^a 375 ^b |
| Earthshine | 160 | 160 | 250 | 250 |
| Earthshine + sun | 190 | 160 | 275 | 250 |
| Collisions | $\sim 5 \times 10^4$ | | 1000 \rightarrow 4000 | |

^aWith Infrared Handbook data. ^bWith AFGL line data.⁷

Table 5 Spectral detection probabilities

| Excitation mechanism | Interferometer | | Radiometer | |
|----------------------|-------------------|-------------------|-------------------|-------------------|
| | 2.7- μ m band | 6.3- μ m band | 2.7- μ m band | 6.3- μ m band |
| Radiative or thermal | $f_T = 0.015$ | 0.013 | 1.00 | 1.00 |
| Collision | $f_C = 0.004$ | 0.004 | 0.74 | 0.57 |

With these widths, the fraction of emission occurring within the spectral bandpasses of the CIRRIS 1A sensors was computed. For the spectrometer (assuming that $\Delta\nu$ is located within the band), this fraction is $f = \Delta\nu/\omega$. For the radiometer, f is the area of overlap between ω and the radiometer bandpass divided by ω . The results are given in Table 5. In use, the values of Q_S , Q_R , and Q_C occurring in the radiation models Eqs. (13) and (16) are replaced with $Q_S f_T$, $Q_R f_T$ and $Q_C f_C$, respectively.

V. Water Outflux

The intensity of observed radiation predicted by these models is directly proportional to the rate of ejection of H₂O molecules from the Shuttle environment. To estimate this rate, the data reported by Carignan and Miller^{9,10} for Shuttle mission STS-4 were used. Most of the measurements were made with a collimated mass spectrometer looking out from the Shuttle bay and sensing the return flux of H₂O to the Shuttle. The return flux is assumed to arise from collisions between H₂O ejected from the Shuttle and ambient atmospheric oxygen atoms. The envelope of return flux data for 140 h of the mission is shown as the shaded regions in Fig. 3. The calibration constant is 10^4 counts/s = 2.1×10^{13} molecules/cm²-s.

Three features are of significance: 1) the width in count rate of the envelope, 2) the strong modulations that occur at MET (mission elapse time) $\approx 25, 55, 75, 95$ and 115 h, and 3) the overall decreasing trend of the data with time. The decreasing trend and width of the envelope were analyzed by drawing the two curves shown in the figure. This is assumed to be the trend of the return flux if the strong modulation did not occur. After subtracting the instrument background count rate, the curves were fitted to double exponential functional forms to obtain

$$F_U(t) = 6.0 \times 10^{13} e^{-t/5.9} + 2.9 \times 10^{12} e^{-t/54}$$

$$F_L(t) = 9.6 \times 10^{12} e^{-t/6.8} + 1.4 \times 10^{12} e^{-t/26}$$

where t is in hours and F is return molecules/cm²-s. These results indicate a relatively fast initial ejection rate (time constant ~ 6 –7 h) that lasts for ~ 20 h followed by a slower rate with a time constant of order 1–2 days.

These two curves are separated by a factor of 6–30, depending on time (the larger value occurring later). This separation, and the corresponding separation between the upper and lower bounds of the envelope of the actual data, is interpreted as caused by the variation of angle of attack between the mass spectrometer axis and the ambient freestream velocity vector. The upper boundary corresponds to looking directly into the atmospheric wind ($\phi = 0$), where the return flux by scattering is largest; the lower curve corresponds to looking at $\phi = 90$ deg

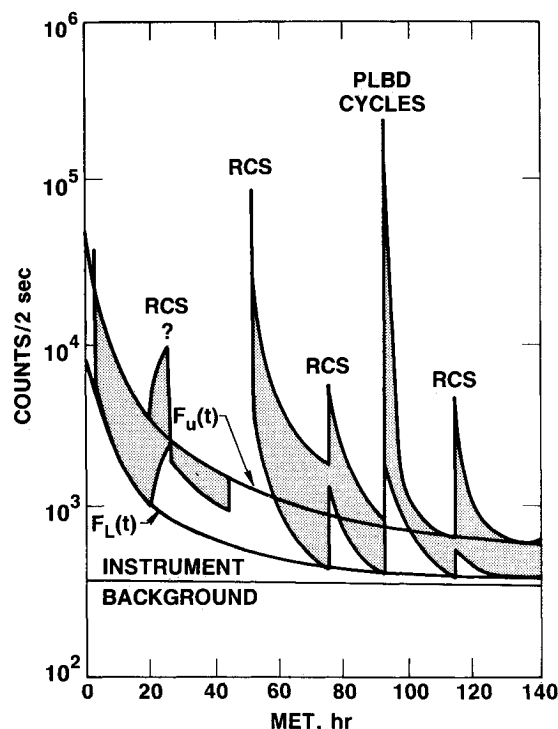


Fig. 3 Envelope of H₂O return flux over the duration of flight of STS-4.⁹

or greater to the wind. The separation factor of 6–30 corresponds well with factors deduced from theoretical analyses. From the Monte Carlo model of Bird,¹¹ the separation factor between $\phi = 0$ and 90 deg predicted for the STS-4 flight conditions is 5.3.

The cause of the large spike modulation is not clearly established. In the 1983 report of these results,⁹ the spikes were attributed to large motor firings on the Shuttle or to a payload door closing event (indicated by RCS and PLBD in Fig. 3). Other measurements,¹² however, show a near instantaneous decrease of return flux when Shuttle motors are turned off. Here, except for the event at 25 h, a decay time of several hours is displayed. The most recent published discussion of these data¹⁰ raises the possibilities of "instrumental artifact" and "outgassing over Shuttle surfaces" as explanations for the long decay times.

Another explanation is that it is the strong peak structure, rather than the width of the envelope, that reflects the dependency on angle of attack with the atmospheric wind direction.

This interpretation is not used here. One feature of the peaks is the near 24 h periodicity of the peaks, suggesting that the peaks may arise from some daily vent activity by the Shuttle crew.

Whatever the cause of the strong modulation and slow decay, it is treated here as real and not an instrumental artifact. The peak value of the return flux for each of these events is listed in Table 6.

For the very short period from MET \approx 45–48 h, direct measurements of H₂O flux away from the Shuttle were made. The mass spectrometer was lifted out of the bay with the remote manipulator and positioned to look back at the Shuttle bay area. Data obtained in this mode are shown in Fig. 4. The dashed lines indicate the range of instrument count rate measured and correspond to 2.2×10^{13} – 4.5×10^{13} molecules/cm²-s. The large off-scale spikes are attributed to thruster firings. The maximum return flux that would have been measured during this time is $F_r \approx 1.2 \times 10^{12}$ molecules/cm²-s. The ratio of the average outflux to maximum return flux is then ~ 30 . This number compares well with the value ~ 68 deduced from the Monte Carlo scattering model of Bird¹¹ for this condition.

From these data and the Monte Carlo scattering model, the following H₂O ejection history is constructed. The underlying Shuttle ejection rate is taken as the upper bound of the unmodulated return flux multiplied by the out-to-return-flux ratio 68 and a 1/2-Shuttle area of 3×10^6 cm². The result is (M in molecules/s, t in h)

$$M = 1.2 \times 10^{22} e^{-t/5.9} + 5.9 \times 10^{20} e^{-t/54}$$

The peak ejection rates are obtained with the same conversion factors and are listed in Table 6. A decay time of 5.9 h is assigned to each spike.

The integral of M (including peaks) over all time indicates a total release into 2π steradians of 2.0×10^{27} molecules (60 kg or 130 lb). The average ejection rate over 140 h is $\bar{M} = 4.0 \times 10^{21}$ molecules/s. The average ejection rate over 140 h, not including peaks, is 7.3×10^{20} molecules/s. The ejection rate at 5.9 h after the largest spike (at 95 h) is 2.2×10^{22} molecules/s. The peak rate itself is 5.3×10^{22} molecules/s. Thus, CIRRIS

Table 6 Peak fluxes for spike events

| MET, h | F , molecules/cm ² -s | | |
|--------|------------------------------------|---------|-------------------|
| | Return | Ejected | M , molecules/s |
| 25 | 9.6(12) | 6.5(14) | 2.0(21) |
| 55 | 1.0(14) | 6.8(15) | 2.0(22) |
| 75 | 6.2(12) | 4.2(14) | 1.3(21) |
| 95 | 2.6(14) | 1.8(16) | 5.3(22) |
| 115 | 5.0(12) | 3.4(14) | 1.0(21) |

1A may have to operate in an environment where the ejection rate of H₂O varies from 10^{20} – 10^{23} molecules/s.

VI. Results

The results of applying the radiation models in the Shuttle altitude range of 200–600 km are presented in Tables 7 and 8 for the 2.7- and 6.3- μ m bands. The contributions from Shuttle excitation (S), radiation excitation (R), and collisional excitation (C) are individually tabulated. The entries are signal-to-noise ratio (STN) where the noise is the NESR of the CIRRIS 1A sensors listed in Table 2. The molecular ejection rate is $M = 1$ molecule/s into 2π steradians. In calculating the collisional contribution, both the quantum mechanical cross sections of Johnson⁴ and the classical cross section results were used, although only the results with Johnson's results are shown in the tables. The classical cross section results may be obtained by multiplying the C column by 15.0 for Table 7 and by 2.92 for Table 8 and resumm for the total contributions.

A few general conclusions can be drawn from these results. In the 2.7- μ m band, the contribution (S) from the initial vibrational energy carried from the Shuttle can be ignored. This might not be the case, however, for a higher Shuttle environment temperature (if the side of the Shuttle containing the sensor field of view were sunlit, e.g.). During the day, the radiation-induced (R) and the collision-induced (C) contributions are each important, with the former dominating at the higher altitudes and the latter dominating at the lower altitudes. At night, the collision-induced (C) contribution dominates at all altitudes. In the 6.3- μ m region, all three contributions are comparable for day or night conditions.

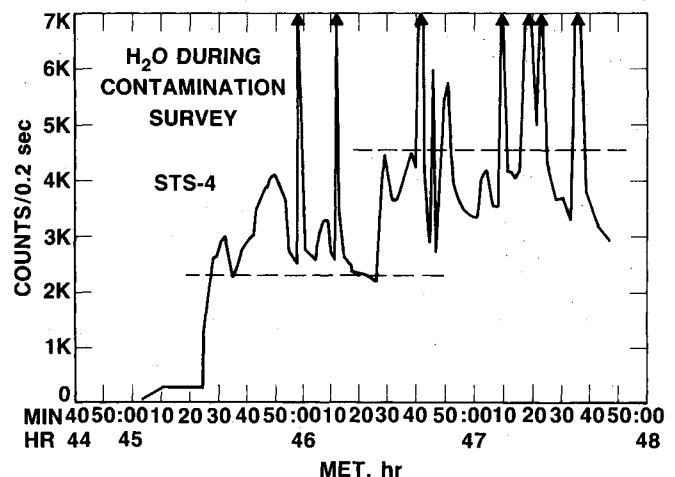


Fig. 4. Measurement of H₂O during flight STS-4.⁹

Table 7 STN ratio for 2.7- μ m band at $M = 1$ molecule/s

| h , km | S | R (day) | R (night) | C | Σ (day) | Σ (night) |
|----------------|----------|-----------|-------------|----------|----------------|------------------|
| Interferometer | | | | | | |
| 200 | 1.8(–26) | 1.3(–23) | 1.9(–26) | 2.3(–22) | 2.4(–22) | 2.3(–22) |
| 300 | 1.8(–26) | 1.3(–23) | 1.8(–26) | 4.6(–23) | 5.8(–23) | 4.6(–23) |
| 400 | 1.8(–26) | 1.3(–23) | 1.7(–26) | 7.5(–24) | 2.0(–23) | 7.5(–24) |
| 500 | 1.8(–26) | 1.3(–23) | 1.6(–26) | 1.6(–24) | 1.4(–23) | 1.6(–24) |
| 600 | 1.8(–26) | 1.3(–23) | 1.5(–26) | 4.3(–25) | 1.3(–23) | 4.6(–25) |
| Radiometer | | | | | | |
| 200 | 7.6(–28) | 5.7(–24) | 8.6(–27) | 3.8(–23) | 4.4(–23) | 3.8(–23) |
| 300 | 7.6(–28) | 5.7(–24) | 8.0(–27) | 2.3(–23) | 2.9(–23) | 2.3(–23) |
| 400 | 7.6(–28) | 5.7(–24) | 7.5(–27) | 6.5(–24) | 1.2(–23) | 6.5(–24) |
| 500 | 7.6(–28) | 5.7(–24) | 7.1(–27) | 1.5(–24) | 7.2(–24) | 1.5(–24) |
| 600 | 7.6(–28) | 5.7(–24) | 6.7(–27) | 4.1(–24) | 6.1(–24) | 4.2(–25) |

S = Shuttle excitation; R = radiation excitation; C = collision excitation; Σ = total contribution.

Table 8 STN ratio for 6.3- μm band at $M = 1$ molecule/s

| h , km | S | R (day) | R (night) | C | Σ (day) | Σ (night) |
|----------------|----------|-----------|-------------|----------|----------------|------------------|
| Interferometer | | | | | | |
| 200 | 2.8(-21) | 7.7(-22) | 7.3(-22) | 3.1(-20) | 3.4(-20) | 3.4(-20) |
| 300 | 2.8(-21) | 7.2(-22) | 6.8(-22) | 6.1(-21) | 9.6(-21) | 9.6(-21) |
| 400 | 2.8(-21) | 6.8(-22) | 6.3(-22) | 1.0(-21) | 4.5(-21) | 4.5(-21) |
| 500 | 2.8(-21) | 6.5(-22) | 6.0(-22) | 2.1(-22) | 3.6(-21) | 3.6(-21) |
| 600 | 2.8(-21) | 6.0(-22) | 5.7(-22) | 5.7(-23) | 3.4(-21) | 3.4(-21) |
| Radiometer | | | | | | |
| 200 | 5.9(-23) | 1.4(-22) | 1.4(-22) | 8.7(-22) | 1.1(-21) | 1.1(-21) |
| 300 | 5.9(-23) | 1.4(-22) | 1.3(-22) | 5.2(-22) | 7.2(-22) | 7.1(-21) |
| 400 | 5.9(-23) | 1.3(-22) | 1.2(-22) | 1.5(-22) | 3.3(-22) | 3.2(-21) |
| 500 | 5.9(-23) | 1.2(-22) | 1.1(-22) | 3.4(-23) | 2.1(-22) | 2.0(-21) |
| 600 | 5.9(-23) | 1.1(-22) | 1.1(-22) | 9.3(-24) | 1.8(-22) | 1.7(-21) |

S = Shuttle excitation; R = radiation excitation; C = collision excitation; Σ = total contribution.

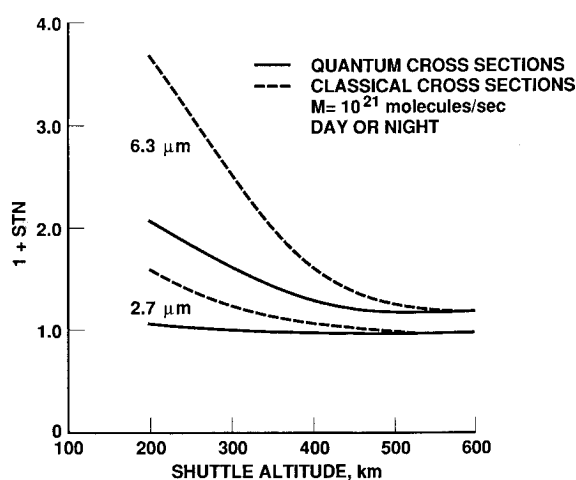


Fig. 5 Effective noise level for CIRRIS 1A radiometer.

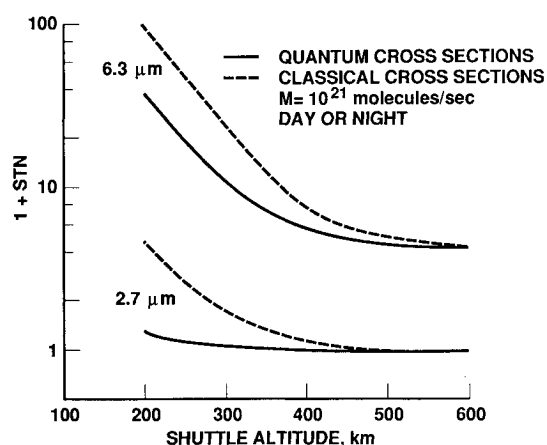


Fig. 6 Effective noise level for CIRRIS 1A interferometer.

In Figs. 5 and 6, results for a moderate H_2O ejection rate of $M = 10^{21}$ molecules/s are shown. The quantity plotted is $1 + \text{STN}(M)$ vs Shuttle altitude. These results show that detection in the 2.7- μm band will not be impaired at any Shuttle altitude if the collision cross sections for inducing radiation in $\text{O} + \text{H}_2\text{O}$ collisions is as small as the quantum mechanical calculations indicate. If the classical cross sections are more accurate, the effective noise level of the sensors may be increased by a factor of 1.2–5 at the lowest Shuttle altitude (200 km). For the 6.3- μm band, a constant impairment is maintained at all altitudes due to the absorption and re-emission of Earthshine radiation (R). The effective noise level of the radiometer is increased by a factor of ~ 1.2 , while the level for the interferometer is increased by ~ 5 . At lower altitudes, these levels are further increased by the effect of collision-induced radiation (C). At 200 km, the effective noise levels are increased by a factor of 4 for the radiometer and 100 for the interferometer. Corresponding results for larger ejection rates can be constructed from the results of Tables 7 and 8.

Acknowledgment

This work was supported by the U.S. Air Force Systems Command, Space Division, under Contract F04701-85-C-0086.

References

- ¹Simpson, J. P. and Witteborn, F. C., "Effect of the Shuttle Contaminant Environment on a Sensitive Infrared Telescope," *Applied Optics*, Vol. 16, Aug. 1977, pp. 2051–2073.
- ²Ahmadjion, M., Smith, D. R. and Stair, A. T., "CIRRIS-A Cryogenic Infrared (IR) Radiance Instrument for Shuttle," *Proceedings of SPIE—The International Society for Optical Engineering*, Vol. 280,

1981, pp. 45–53.

³U.S. *Standard Atmosphere*, 1976, National Oceanic and Atmospheric Administration, Washington, D.C., Oct. 1976.

⁴Johnson, B. R., "A Quantum Mechanical Investigation of Vibrational Energy Transfer in $\text{O}(\text{P}) + \text{H}_2\text{O}$ Collisions," *Journal of Chemical Physics*, Vol. 84, Jan. 1986, pp. 176–180.

⁵Redmon, M. J., Redmon, L. T., and Garrett, B. C., "Collisional Excitation Cross Sections," Air Force Rocket Propulsion Laboratory, Edwards Air Force Base, CA, AFRPL TR-84-030, Aug. 1984; also, Redmon, M. J. et al., "Collisional Excitation of H_2O by O-Atom Impact: Classical Dynamics on an Accurate Ab Initio Potential Energy Surface," *Potential Energy Surfaces and Dynamics Calculations*, edited by D. G. Truhlar, Plenum Press, New York, 1981, pp. 771–803.

⁶Ludwig, C. B., Malkmus, W., Reardon, J. E., and Thompson, J. A. L., "Handbook of Infrared Radiation From Combustion Gases," edited by R. Goulard and J. A. L. Thompson, NASA SP-3080, 1973.

⁷Young, S. J., "Band Model Parameters for the 2.7- μm Bands of H_2O and CO_2 in the 100 to 3000 K Temperature Range," The Aerospace Corporation, El Segundo, CA, TR-0076(6970)-4, July 1975.

⁸Kolb, C. E. and Elgin, J. B., "Classical Calculation of NH_3 and H_2O Rotational Excitation in Energetic Collisions with Atomic Oxygen," *Journal of Chemical Physics*, Vol. 66, Jan. 1977, pp. 119–124.

⁹Carignan, G. R. and Miller, E. R., "Mass Spectrometer in STS-2, -3, -4 Induced Environment Contamination Monitor Summary Report," NASA TM-82524, Feb. 1983.

¹⁰Green, B. D., Caledonia, G. E., and Wilkerson, T. D., "The Shuttle Environment: Gases, Particulates, and Glow," *Journal of Spacecraft and Rockets*, Vol. 22, Sept.–Oct. 1985, pp. 500–511.

¹¹Bird, G. A., "Spacecraft Outgas Ambient Flow Interactions," *Journal of Spacecraft and Rockets*, Vol. 18, Jan.–Feb. 1981, pp. 31–35.

¹²Narcisi, R., Trzcinski, E., Federico, G., Wlodyka, L., and Delorey, D., "The Gaseous and Plasma Environment around Space Shuttle," *Proceedings of the AIAA Shuttle Environment and Operations Meeting*, AIAA, New York, 1983, pp. 183–190.